

Measurement of the $B \rightarrow K^* \gamma$ Branching Fractions and Asymmetries

M. Nakao,⁶ K. Abe,⁶ K. Abe,³⁸ T. Abe,⁶ I. Adachi,⁶ H. Aihara,⁴⁰ M. Akatsu,¹⁹ Y. Asano,⁴⁵ T. Aso,⁴⁴ V. Aulchenko,¹ T. Aushev,¹⁰ S. Bahinipati,³ A. M. Bakich,³⁵ Y. Ban,²⁹ A. Bay,¹⁵ U. Bitenc,¹¹ I. Bizjak,¹¹ A. Bondar,¹ A. Bozek,²³ M. Bračko,^{17,11} T. E. Browder,⁵ P. Chang,²² Y. Chao,²² K.-F. Chen,²² B. G. Cheon,³⁴ Y. Choi,³⁴ A. Chuvikov,³⁰ S. Cole,³⁵ M. Danilov,¹⁰ M. Dash,⁴⁷ L. Y. Dong,⁸ J. Dragic,¹⁸ A. Drutskoy,¹⁰ S. Eidelman,¹ V. Eiges,¹⁰ Y. Enari,¹⁹ F. Fang,⁵ S. Fratina,¹¹ N. Gabyshev,⁶ A. Garmash,³⁰ T. Gershon,⁶ G. Gokhroo,³⁶ B. Golob,^{16,11} H. Hayashii,²⁰ M. Hazumi,⁶ T. Higuchi,⁶ L. Hinz,¹⁵ T. Hokuue,¹⁹ Y. Hoshi,³⁸ W.-S. Hou,²² Y. B. Hsiung,^{22,*} T. Iijima,¹⁹ K. Inami,¹⁹ A. Ishikawa,⁶ H. Ishino,⁴¹ R. Itoh,⁶ H. Iwasaki,⁶ M. Iwasaki,⁴⁰ J. H. Kang,⁴⁹ J. S. Kang,¹³ N. Katayama,⁶ H. Kawai,² T. Kawasaki,²⁵ H. Kichimi,⁶ H. J. Kim,⁴⁹ J. H. Kim,³⁴ S. K. Kim,³³ T. H. Kim,⁴⁹ K. Kinoshita,³ P. Koppenburg,⁶ S. Korpar,^{17,11} P. Križan,^{16,11} P. Krokovny,¹ A. Kuzmin,¹ Y.-J. Kwon,⁴⁹ J. S. Lange,^{4,31} S. H. Lee,³³ T. Lesiak,²³ J. Li,³² A. Limosani,¹⁸ S.-W. Lin,²² J. MacNaughton,⁹ G. Majumder,³⁶ F. Mandl,⁹ T. Matsumoto,⁴² Y. Mikami,³⁹ W. Mitaroff,⁹ K. Miyabayashi,²⁰ H. Miyake,²⁷ H. Miyata,²⁵ D. Mohapatra,⁴⁷ G. R. Moloney,¹⁸ T. Mori,⁴¹ T. Nagamine,³⁹ Y. Nagasaka,⁷ E. Nakano,²⁶ H. Nakazawa,⁶ K. Neichi,³⁸ S. Nishida,⁶ O. Nitoh,⁴³ T. Nozaki,⁶ S. Ogawa,³⁷ T. Ohshima,¹⁹ T. Okabe,¹⁹ S. Okuno,¹² S. L. Olsen,⁵ W. Ostrowicz,²³ P. Pakhlov,¹⁰ H. Palka,²³ H. Park,¹⁴ N. Parslow,³⁵ L. S. Peak,³⁵ L. E. Piilonen,⁴⁷ F. J. Ronga,⁶ M. Rozanska,²³ H. Sagawa,⁶ S. Saitoh,⁶ Y. Sakai,⁶ T. R. Sarangi,⁴⁶ O. Schneider,¹⁵ J. Schümann,²² C. Schwanda,⁹ A. J. Schwartz,³ S. Semenov,¹⁰ K. Senyo,¹⁹ R. Seuster,⁵ M. E. Sevier,¹⁸ B. Shwartz,¹ J. B. Singh,²⁸ N. Soni,²⁸ R. Stamen,⁶ S. Stanič,^{45,†} M. Starič,¹¹ T. Sumiyoshi,⁴² S. Suzuki,⁴⁸ O. Tajima,³⁹ F. Takasaki,⁶ M. Tanaka,⁶ G. N. Taylor,¹⁸ Y. Teramoto,²⁶ T. Tomura,⁴⁰ T. Tsuboyama,⁶ T. Tsukamoto,⁶ S. Uehara,⁶ T. Uglov,¹⁰ S. Uno,⁶ Y. Ushiroda,⁶ G. Varner,⁵ K. E. Varvell,³⁵ C. C. Wang,²² C. H. Wang,²¹ M.-Z. Wang,²² M. Watanabe,²⁵ Y. Yamada,⁶ A. Yamaguchi,³⁹ Y. Yamashita,²⁴ M. Yamauchi,⁶ Heyoung Yang,³³ J. Ying,²⁹ Y. Yusa,³⁹ C. C. Zhang,⁸ J. Zhang,⁶ Z. P. Zhang,³² V. Zhilich,¹ T. Ziegler,³⁰ and D. Žontar^{16,11}

(The Belle Collaboration)

¹*Budker Institute of Nuclear Physics, Novosibirsk*

²*Chiba University, Chiba*

³*University of Cincinnati, Cincinnati, Ohio 45221*

⁴*University of Frankfurt, Frankfurt*

⁵*University of Hawaii, Honolulu, Hawaii 96822*

⁶*High Energy Accelerator Research Organization (KEK), Tsukuba*

⁷*Hiroshima Institute of Technology, Hiroshima*

⁸*Institute of High Energy Physics, Chinese Academy of Sciences, Beijing*

⁹*Institute of High Energy Physics, Vienna*

¹⁰*Institute for Theoretical and Experimental Physics, Moscow*

¹¹*J. Stefan Institute, Ljubljana*

¹²*Kanagawa University, Yokohama*

¹³*Korea University, Seoul*

¹⁴*Kyungpook National University, Taegu*

¹⁵*Swiss Federal Institute of Technology of Lausanne, EPFL, Lausanne*

¹⁶*University of Ljubljana, Ljubljana*

¹⁷*University of Maribor, Maribor*

¹⁸*University of Melbourne, Victoria*

¹⁹*Nagoya University, Nagoya*

²⁰*Nara Women's University, Nara*

- ²¹*National United University, Miao Li*
²²*Department of Physics, National Taiwan University, Taipei*
²³*H. Niewodniczanski Institute of Nuclear Physics, Krakow*
²⁴*Nihon Dental College, Niigata*
²⁵*Niigata University, Niigata*
²⁶*Osaka City University, Osaka*
²⁷*Osaka University, Osaka*
²⁸*Panjab University, Chandigarh*
²⁹*Peking University, Beijing*
³⁰*Princeton University, Princeton, New Jersey 08545*
³¹*RIKEN BNL Research Center, Upton, New York 11973*
³²*University of Science and Technology of China, Hefei*
³³*Seoul National University, Seoul*
³⁴*Sungkyunkwan University, Suwon*
³⁵*University of Sydney, Sydney NSW*
³⁶*Tata Institute of Fundamental Research, Bombay*
³⁷*Toho University, Funabashi*
³⁸*Tohoku Gakuin University, Tagajo*
³⁹*Tohoku University, Sendai*
⁴⁰*Department of Physics, University of Tokyo, Tokyo*
⁴¹*Tokyo Institute of Technology, Tokyo*
⁴²*Tokyo Metropolitan University, Tokyo*
⁴³*Tokyo University of Agriculture and Technology, Tokyo*
⁴⁴*Toyama National College of Maritime Technology, Toyama*
⁴⁵*University of Tsukuba, Tsukuba*
⁴⁶*Utkal University, Bhubaneswer*
⁴⁷*Virginia Polytechnic Institute and State University, Blacksburg, Virginia 24061*
⁴⁸*Yokkaichi University, Yokkaichi*
⁴⁹*Yonsei University, Seoul*

We report measurements of the radiative decay $B \rightarrow K^*\gamma$. The analysis is based on a data sample containing 85.0×10^6 B meson pairs collected by the Belle detector at the KEKB storage ring. We measure branching fractions of $\mathcal{B}(B^0 \rightarrow K^{*0}\gamma) = (4.01 \pm 0.21 \pm 0.17) \times 10^{-5}$ and $\mathcal{B}(B^+ \rightarrow K^{*+}\gamma) = (4.25 \pm 0.31 \pm 0.24) \times 10^{-5}$, where the first and second errors are statistical and systematic, respectively. The isospin asymmetry between B^0 and B^+ decay widths is measured to be $\Delta_{0+} = +0.012 \pm 0.044 \pm 0.026$. We search for a partial rate asymmetry between CP conjugate modes, and find $A_{CP}(B \rightarrow K^*\gamma) = -0.015 \pm 0.044 \pm 0.012$.

PACS numbers: 13.40.Hq, 14.40.Nd

INTRODUCTION

One decade after the first observation of exclusive $B \rightarrow K^*\gamma$ decays by CLEO in 1993 [1], this process continues to be a subject of considerable interest. The size of the decay rate itself provides only a mild constraint on extensions to the Standard Model (SM), because SM predictions for exclusive rates suffer from large ($\sim 30\%$) and model dependent form factor uncertainties [2]. Of more interest are asymmetries, where theoretical uncertainties largely cancel. The isospin asymmetry between the charged and neutral $B \rightarrow K^*\gamma$ decay widths is predicted to be $+5$ to 10% in the SM, while in some SM extensions it may have an opposite sign [3]. A measurement of the partial rate asymmetry between CP conjugate modes is another interesting subject; here the SM expectation is much less than 1% and any large asymmetry would be an indication of non-SM effects. In this report, we present new measurements of the $B \rightarrow K^*\gamma$ branching fractions, and isospin and charge asymmetries.

DATASET AND APPARATUS

The data sample used in this analysis contains $(85.0 \pm 0.5) \times 10^6$ B meson pairs, corresponding to an integrated luminosity of 78 fb^{-1} , collected at the $\Upsilon(4S)$ resonance by the Belle detector at the KEKB storage ring. KEKB is a double-ring asymmetric-energy e^+e^- storage ring (3.5 GeV on 8 GeV) [4]. We also use an off-resonance data sample of 8.3 fb^{-1} collected at a center-of-mass (CM) energy that is 60 MeV below the $\Upsilon(4S)$ resonance.

The Belle detector is a large-solid-angle magnetic spectrometer that consists of a three-layer silicon vertex detector (SVD), a 50-layer central drift chamber (CDC), an array of aerogel threshold Cherenkov counters (ACC), a barrel-like arrangement of time-of-flight scintillation counters (TOF), and an electromagnetic calorimeter (ECL) comprised of CsI(Tl) crystals located inside a super-conducting solenoid coil that provides a 1.5 T magnetic field. An iron flux-return located outside of the coil is instrumented to detect K_L^0 mesons and to identify

muons (KLM). The detector is described in detail elsewhere [5].

SIGNAL RECONSTRUCTION

The analysis is performed by reconstructing B meson candidates that include a high energy primary photon and a K^* resonance reconstructed in one of four final states: $K^+\pi^-$, $K_S^0\pi^0$, $K_S^0\pi^+$, and $K^+\pi^0$. Here and throughout this report, K^* denotes the $K^*(892)$, and the inclusion of charge conjugate modes is implied unless otherwise stated.

Photon (γ) candidates are reconstructed from isolated clusters in the ECL that have no corresponding charged track, and a shower shape that is consistent with that of a photon. The photon energy is calculated from the sum of energies in crystals with more than 0.5 MeV energy deposited around the central cell. Photons in the energy range $1.8 \text{ GeV} < E_\gamma^* < 3.4 \text{ GeV}$ in the barrel region of the ECL ($33^\circ < \theta_\gamma < 128^\circ$) are selected as primary photon candidates from B decay; here E_γ^* is the photon energy in the CM frame and θ_γ is the polar angle in the laboratory frame. (We use variables calculated both in the CM frame and laboratory frame: variables defined in the CM frame are labeled with an asterisk.) In order to reduce the backgrounds from π^0 and η mesons from continuum light quark-pair production ($e^+e^- \rightarrow q\bar{q}$, $q = u, d, s, c$), we impose two additional requirements on the primary photon. One is the explicit removal of π^0 (η) candidates by requiring the invariant mass of the primary photon and any other photon with an energy greater than 30 MeV (200 MeV) to be outside of a window of $\pm 18 \text{ MeV}/c^2$ ($\pm 32 \text{ MeV}/c^2$) around the nominal π^0 (η) mass. These correspond to $\pm 3\sigma$ windows, where σ is the mass resolution. This set of criteria is referred to as the π^0/η veto. The other requirement is the removal of the clusters that are not fully consistent with an isolated electromagnetic shower. We require the ratio of the energy deposition in 3×3 cells to that in 5×5 cells around the maximum energy ECL cell of the cluster ($E_{9/25}$) to be greater than 0.95, which retains 95% of the signal photons.

Charged pions (π^\pm) and kaons (K^\pm) are reconstructed as tracks in the CDC and SVD. The tracks are required to originate from the interaction region by requiring that they have radial impact parameters relative to the run-averaged measured interaction point of less than 1.5 cm. We determine the pion (L_π) and kaon (L_K) likelihoods from the ACC response, the specific ionization (dE/dx) measurement in the CDC and the TOF flight-time measurement for each track, and form a likelihood ratio $L_{K/\pi} = L_K/(L_\pi + L_K)$ to separate pions and kaons. We require $L_{K/\pi} > 0.6$ for kaons, which gives an efficiency of 86% for kaons, and $L_{K/\pi} < 0.9$ for pions, which gives an efficiency of 96% for pions. In addition, we remove kaon

and pion candidates if they are consistent with being electrons based on the ECL, dE/dx , and ACC information.

Neutral pions (π^0) are formed from two photons with invariant masses within $\pm 16 \text{ MeV}$ (3σ) of the π^0 mass; the photon momenta are then recalculated with a π^0 mass constraint. The π^0 mass resolution is better than that for the π^0/η veto where the photon energies are highly asymmetric. We require each photon energy to be greater than 50 MeV, and the cosine of the angle between the two photons ($\cos\theta_{\gamma\gamma}$) to be greater than 0.5. This angle requirement is almost equivalent to selecting π^0 s with momentum above 0.5 GeV/ c ; it retains about 90% of the signal π^0 s while rejecting 43% of the π^0 candidates in the background.

Neutral kaons (K_S^0) are reconstructed from two oppositely charged pions that have invariant masses within $\pm 10 \text{ MeV}$ (3σ) of the K_S^0 mass; the pion momenta are then recalculated with a K_S^0 vertex constraint. We impose additional criteria based on the radial impact parameters of the pions (δr), the distance between the closest approaches of the pions along the beam direction (δz), the distance of the vertex from the interaction point (l), and the azimuthal angle difference between the vertex direction and the K_S^0 momentum direction ($\delta\phi$). These variables are combined as follows: for $p(K_S^0) < 0.5 \text{ GeV}/c$, $\delta z < 8 \text{ mm}$, $\delta r > 0.5 \text{ mm}$, and $\delta\phi < 0.3 \text{ rad}$ are required; for $0.5 \text{ GeV}/c < p(K_S^0) < 1.5 \text{ GeV}/c$, $\delta z < 18 \text{ mm}$, $\delta r > 0.3 \text{ mm}$, $\delta\phi < 0.1 \text{ rad}$, and $l > 0.8 \text{ mm}$ are required; and for $p(K_S^0) > 1.5 \text{ GeV}/c$, $\delta z < 24 \text{ mm}$, $\delta r > 0.2 \text{ mm}$, $\delta\phi < 0.03 \text{ rad}$, and $l > 2.2 \text{ mm}$ are required. This set of criteria retains about 80% of the signal K_S^0 .

We form a B candidate from a primary photon candidate and a K^* candidate, which is a $K\pi$ system with an invariant mass $M(K\pi)$ within $\pm 75 \text{ MeV}/c^2$ of the K^* mass. In order to separate the B candidate from backgrounds, we form two kinematic variables: the beam-energy constrained mass $M_{\text{bc}} = \sqrt{(E_{\text{beam}}^*/c^2)^2 - |\vec{p}_B^*/c|^2}$ and the energy difference $\Delta E = E_B^* - E_{\text{beam}}^*$, where E_{beam}^* is the beam energy, and E_B^* and \vec{p}_B^* are the energy and momentum, respectively, of the B candidate in the CM frame. The energy E_B^* is calculated as $E_B^* = E_\gamma^* + E_{K^*}^*$; the momentum \vec{p}_B^* is calculated without using the absolute value of the photon momentum according to

$$\vec{p}_B^* = \vec{p}_{K^*}^* + \frac{\vec{p}_\gamma^*}{|\vec{p}_\gamma^*|} \times (E_{\text{beam}}^* - E_{K^*}^*), \quad (1)$$

since the K^* momentum and the beam energy are determined with substantially better precision than that of the primary photon.

We use M_{bc} as the primary distribution to extract the signal yield. For modes without a π^0 , we use a Gaussian function with a width of $(2.73 \pm 0.04) \text{ MeV}/c^2$ to model the signal; for modes with a π^0 , we use an empirical formula to reproduce the asymmetric ECL energy response

(known as the Crystal Ball line shape [6]), whose effective width is $(3.35 \pm 0.10) \text{ MeV}/c^2$. The peak positions and widths are primarily determined using Monte Carlo (MC) samples, and corrected for the measured differences in the beam-energy and its spread between data and MC using a $B^- \rightarrow D^0 \pi^-$ sample. The ΔE signal distribution also has a large tail on the negative ΔE side due to the asymmetric ECL energy response. For the modes without a π^0 , we use a Crystal Ball line shape; for the modes with a π^0 , we convolve an additional Gaussian resolution function to describe a broader width and add a broad Gaussian component for the small tail in the positive ΔE side. These shapes are determined using MC samples. We select candidates with $-200 \text{ MeV} < \Delta E < 100 \text{ MeV}$ to accommodate the asymmetric ΔE signal shape. We define a ΔE sideband as $100 \text{ MeV} < \Delta E < 400 \text{ MeV}$, where no signal is expected, to study the M_{bc} distribution of the background. There is no background that makes a peak in this ΔE sideband. We require $M_{bc} > 5.270 \text{ GeV}/c^2$ when the ΔE distribution is examined. We define $5.227 \text{ GeV}/c^2 < M_{bc} < 5.263 \text{ GeV}/c^2$ as an M_{bc} sideband that is used to study the ΔE distribution of the background.

BACKGROUND SUPPRESSION

The main background source is continuum $q\bar{q}$ production including the initial state radiation process $e^+e^- \rightarrow q\bar{q}\gamma$. We reduce this background by exploiting the topological event shape differences: B meson pairs decay almost at rest in the CM frame and thus the final state particles are distributed nearly isotropically; $q\bar{q}$ pairs are produced back-to-back with multi-GeV/ c momenta in both hemispheres and, thus, tend to be more two-jet like.

We define a Fisher discriminant (F) [7] from modified Fox-Wolfram moments [8],

$$F = \alpha_2 R_2^{so} + \alpha_4 R_4^{so} + \sum_{l=1}^4 \beta_l R_l^{oo}, \quad (2)$$

where α_l, β_l are coefficients that are selected to provide the maximum discrimination between the signal and the continuum background. The modified Fox-Wolfram moments are defined as

$$R_l^{so} = \frac{\sum_{i,\gamma} |\vec{p}'_i| |\vec{p}'_\gamma| P_l(\cos \theta'_{i\gamma})}{\sum_{i,\gamma} |\vec{p}'_i| |\vec{p}'_\gamma|}, \quad (3)$$

$$R_l^{oo} = \frac{\sum_{i,j} |\vec{p}'_i| |\vec{p}'_j| P_l(\cos \theta'_{ij})}{\sum_{i,j} |\vec{p}'_i| |\vec{p}'_j|},$$

where the indices i, j indicate the charged tracks (with a π^+ mass hypothesis) and photons that are not used to form the B candidate, and the index γ corresponds to the primary photon. The variables θ'_{ij} and $\theta'_{i\gamma}$ are the

opening angles between two momentum vectors, and P_l is the l -th Legendre polynomial function. The momenta (\vec{p}') and angles (θ') are calculated in the candidate B rest frame (denoted as primed variables), since the selection efficiency with this variable has a smaller correlation with M_{bc} than that calculated in the CM frame.

As an additional discriminant, we use the cosine of the CM polar angle of the candidate B flight direction, $\cos \theta_B^*$. The $\cos \theta_B^*$ distribution is $1 - \cos^2 \theta_B^*$ for B production from $e^+e^- \rightarrow \Upsilon(4S)$, and is found to be flat for the continuum background.

We combine these two discriminants into a likelihood ratio,

$$\mathcal{L}_{\text{cont}} = \frac{L_S}{L_S + L_B}, \quad (4)$$

$$L_S = P_S^F \times P_S^{\text{cosB}}, \quad L_B = P_B^F \times P_B^{\text{cosB}},$$

where P^F and P^{cosB} are the probability density functions (PDF) for the Fisher and the B flight direction, and the indices S and B denote the signal and background. For P_S^{cosB} and P_B^{cosB} , we use $\frac{3}{2}(1 - \cos^2 \theta_B^*)$ and $\frac{1}{2}$, respectively. For P_S^F and P_B^F , we model the shape by fitting the signal and continuum background MC distributions with asymmetric Gaussian functions for each of the four $B \rightarrow K^* \gamma$ channels.

The value of $\mathcal{L}_{\text{cont}}$ ranges between 0 and 1. We optimize the minimum $\mathcal{L}_{\text{cont}}$ requirement to provide the largest value of $N_S/\sqrt{N_S + N_B}$, where N_S and N_B are the expected signal and background yields for 85.0×10^6 B meson pairs assuming previously measured $B \rightarrow K^* \gamma$ branching fraction values [9, 10, 11]. Although there is a slight mode dependence in the optimal value, we apply the same requirement, $\mathcal{L}_{\text{cont}} > 0.65$, which is close to the optimal point for each mode. This requirement retains 73% of signal events while rejecting 90% of continuum background events.

The remaining continuum background is distinguished by fits to the M_{bc} distribution. The continuum background is modeled with a threshold function (known as the ARGUS function [12]),

$$f_{\text{cont}}(M_{bc}) = N \times M_{bc} \times \sqrt{1 - \left(\frac{M_{bc}}{E_{\text{beam}}^*}\right)^2} \times \exp \left\{ \alpha \left[1 - \left(\frac{M_{bc}}{E_{\text{beam}}^*}\right)^2 \right] \right\}, \quad (5)$$

where N is a normalization factor and α is an empirical shape parameter. We determine the shape parameter from the ΔE sideband data, since there is no significant difference between the background shapes in the ΔE sideband and the signal region for off-resonance data and MC events. The results are consistent for data and MC, and for the different $B \rightarrow K^* \gamma$ channels. We use the

same background shape parameter α for all the $B \rightarrow K^*\gamma$ channels. For ΔE , the background shape is parameterized as a linear function and determined from M_{bc} side-band data.

Major background contributions from B decays are from cross-feeds between charged and neutral $B \rightarrow K^*\gamma$ decays, $B \rightarrow (K^*\pi + K\rho)\gamma$ [13], $B \rightarrow K^*\eta$ [14] and the unmeasured mode $B \rightarrow K^*\pi^0$ [15] for which we assume half of the upper limit as the branching fraction with a 100% error. These backgrounds peak in M_{bc} around the signal with a slightly larger tail, and have a broad peak in ΔE at negative values. We model these backgrounds and other B decay backgrounds with a smoothed histogram generated from a large MC sample.

SIGNAL EXTRACTION

We extract signal yields in each of the four final states using a one-dimensional binned likelihood fit. The M_{bc} distributions are modeled as a sum of three components: the signal, the continuum background and the B decay backgrounds that are described in the previous sections. Figure 1 shows the result of the fits; clear signals are seen in all four final states. The size of the B decay background component, which is seen as a slight enhancement of the background shape under the signal peak, is fixed in the fitting procedure. We vary the B decay background components by the errors on their branching fractions to evaluate the systematic error due to their uncertainties. We also vary the continuum background shape, E_{beam}^* , the B meson mass, and the M_{bc} resolution by their errors to evaluate the systematic errors on the signal and background PDFs. We use a quadratic sum of the variations in the signal yield with these tests as the systematic error on the signal yield.

A similar fitting procedure is performed for the ΔE distributions as shown in Fig. 2. The ΔE yields are obtained by integrating the fit results from -0.2 GeV to 0.1 GeV to allow a comparison with the M_{bc} results. The fit result for each mode is in agreement with the M_{bc} result as given in Table I. In this analysis, the ΔE distribution is not as reliable as M_{bc} since we have to consider a wide ΔE range where the background contribution from B decays is larger than that for M_{bc} , and ΔE shapes for both signal and background may have large uncertainties that are not fully evaluated due to lack of suitable control samples. Thus we base our signal yields on the M_{bc} fits.

The $M(K\pi)$ invariant mass spectrum, before applying the $|M(K\pi) - M_{K^*}| < 75$ MeV/ c^2 requirement, gives discrimination of the K^* signal from resonances such as $K_2^*(1430)$ and $K^*(1410)$, or a non-resonant $K\pi\gamma$ component. In order to examine the spectrum, we divide the data below $M(K\pi) = 2.0$ GeV/ c^2 into 50 MeV/ c^2 wide bins and extract the signal yield for each bin from a fit to the M_{bc} distribution, using the same fitting procedure

described above. We veto the $D^0 \rightarrow K^-\pi^+$ and $D^0 \rightarrow K_S^0\pi^0$ contributions from $\bar{B}^0 \rightarrow D^0\pi^0$ and $\bar{B}^0 \rightarrow D^0\eta$ backgrounds by requiring $|M(K\pi) - M_{D^0}| > 20$ MeV/ c^2 for the $K^{*0}\gamma$ modes. Other B decay backgrounds that may peak in M_{bc} are included as a background component in each fit. A χ^2 fit is then performed to the $M(K\pi)$ spectrum using a sum of K^* , $K_2^*(1430)$ and $K^*(1410)$ resonances and a non-resonant component without taking into account possible interference effects. The fit results are shown in Fig. 3. For these resonances, we use relativistic Breit-Wigner functions with the nominal masses and widths convolved with a Gaussian resolution function. In addition to the K^* peak, we find a significant $K_2^*(1430)$ peak, while the $K^*(1410)$ component is consistent with zero. The K^* signal yields within the ± 75 MeV/ c^2 window are consistent with the M_{bc} results as given in Table I. In all cases, the background contributions from $K^*(1410)$ and $K_2^*(1430)$ within the K^* mass window are less than one event including their errors. The non-resonant contribution is modeled with the inclusive X_s mass spectrum of Ref. [16]. We find 5.9 ± 2.3 and 6.4 ± 1.9 events under the peak of K^{*0} and K^{*+} , corresponding to $(1.2 \pm 0.5)\%$ and $(2.4 \pm 0.4)\%$ of the signal yields, respectively. We include these yields into the systematic errors instead of subtracting the contributions, since they could also be due to a bias from other high mass resonances such as $K^*(1680)$ that hardly contribute to the K^* mass peak.

The K^* decay helicity angle, θ_{hel} , defined as the angle between the kaon and the B meson directions in the rest frame of the $K\pi$ system, provides discrimination of the spin-1 signal from other spin states. The $\cos\theta_{\text{hel}}$ distribution, shown in Fig. 4, is obtained by dividing the data into bins of 0.1 in $\cos\theta_{\text{hel}}$ and fitting their M_{bc} distributions. The B decay backgrounds that peak in M_{bc} and follow a $\cos^2\theta_{\text{hel}}$ structure due to the pseudoscalar to pseudoscalar-vector nature of the decay are included as a background component in each fit. The $K^*\gamma$ signal has a $1 - \cos^2\theta_{\text{hel}}$ distribution. In order to model a slight distortion due to non-uniform tracking, particle identification and π^0/K_S^0 reconstruction efficiencies, we use a fourth order polynomial function that is constrained to zero at $\cos\theta_{\text{hel}} = \pm 1$. We also add a flat component modified with the same slight distortion, which turns out to be consistent with zero. The fit result is in agreement with the spin-1 signal.

We obtain a consistent set of signal yields from three different distributions, M_{bc} , ΔE , $M(K\pi)$ as summarized in Table I. Both the $M(K\pi)$ and $\cos\theta_{\text{hel}}$ distributions suggest that the contributions from other resonances and non-resonant decays can be neglected. We conclude that the signal yields obtained with the M_{bc} fit are essentially entirely due to $B \rightarrow K^*\gamma$ decays.

BRANCHING FRACTIONS

The reconstruction efficiencies are primarily obtained from signal MC samples. The selection criteria are divided into ten categories, and the systematic error for each of them is evaluated with an independent control sample. The results are summarized in Table II.

The uncertainty in the photon detection efficiency is evaluated with a sample of radiative Bhabha events. For the tracking efficiency, we quote an error from a comparison of the partially reconstructed $D^{*+} \rightarrow D^0\pi^+$, $D^0 \rightarrow K_S^0\pi^+\pi^-$ yield with the fully reconstructed one. For the charged kaon identification, we evaluate the systematic error from a comparison between the efficiencies obtained from kinematically selected $D^{*+} \rightarrow D^0\pi^+$, $D^0 \rightarrow K^-\pi^+$ and $\phi \rightarrow K^+K^-$ decays in data and MC. Similarly for the charged pion identification, we compare the efficiency for the same D^{*+} sample with that obtained from $K_S^0 \rightarrow \pi^+\pi^-$ to evaluate the systematic error. The uncertainty in the K_S^0 reconstruction is obtained from a comparison between $D^+ \rightarrow K_S^0\pi^+$ with $D^+ \rightarrow K^-\pi^+\pi^+$ in $D^{*+} \rightarrow D^+\pi^0$ decays. The uncertainty in the π^0 reconstruction efficiency is evaluated from a comparison of $\eta \rightarrow \pi^0\pi^0\pi^0$ to $\eta \rightarrow \gamma\gamma$ and $\eta \rightarrow \pi^+\pi^-\pi^0$ in data and MC. The efficiencies for the π^0/η veto and the likelihood ratio requirement are evaluated together, using a $B \rightarrow D\pi^-$ control sample that includes the decay channels $B^- \rightarrow D^0\pi^-$, $D^0 \rightarrow K^-\pi^+$ and $\bar{B}^0 \rightarrow D^+\pi^-$, $D^+ \rightarrow K^-\pi^+\pi^+$. We calculate M_{bc} as we do for $B \rightarrow K^*\gamma$, i.e. without using the absolute value of the π^- momentum. For the π^0/η veto, we assume the π^- is a massless particle and scale the momentum by a factor of 1.1 to make the average π^- momentum equal that of the photons for $B \rightarrow K^*\gamma$. We then combine this massless π^- with all photon candidates and reject the event if the same π^0/η veto criteria are satisfied, and compare the results between data and MC control samples. The effect of the $M(K\pi)$ requirement is evaluated by taking into account the K^* form factor and the detector resolution effects into the Breit-Wigner shape.

Using these reconstruction efficiencies, we obtain the branching fractions for each of the four modes as summarized in Table III. We add the signal yields and the efficiencies for two modes of each of neutral and charged B decays, and obtain

$$\begin{aligned} \mathcal{B}(B \rightarrow K^{*0}\gamma) &= (4.01 \pm 0.21 \pm 0.17) \times 10^{-5} \\ \mathcal{B}(B \rightarrow K^{*+}\gamma) &= (4.25 \pm 0.31 \pm 0.24) \times 10^{-5}, \end{aligned} \quad (6)$$

where the first and the second errors are statistical and systematic, respectively. We assume an equal production rate for $B^0\bar{B}^0$ and B^+B^- from the $\Upsilon(4S)$ resonance.

The isospin asymmetry,

$$\Delta_{0+} = \frac{(\tau_{B^+}/\tau_{B^0})\mathcal{B}(B^0 \rightarrow K^{*0}\gamma) - \mathcal{B}(B^+ \rightarrow K^{*+}\gamma)}{(\tau_{B^+}/\tau_{B^0})\mathcal{B}(B^0 \rightarrow K^{*0}\gamma) + \mathcal{B}(B^+ \rightarrow K^{*+}\gamma)}, \quad (7)$$

is then calculated from these results. We use the world average value of $\tau_{B^+}/\tau_{B^0} = 1.086 \pm 0.017$ [14]. We assume that the systematic error on the photon detection cancels. The systematic error on the $\mathcal{L}_{\text{cont}}$ and π^0/η veto requirements is estimated to be 0.013 in Δ_{0+} from a comparison of the \bar{B}^0 and B^- subsets of the $B \rightarrow D\pi^-$ control sample. We find the systematic error due to the $M(K\pi)$ requirement is negligible. Correlations between the systematic errors for the charged pion and kaon tracking and particle identification, and the π^0 and K_S^0 reconstruction efficiencies are taken into account. Systematic errors on the fitting procedures are assumed to be uncorrelated.

The result is

$$\Delta_{0+} = +0.012 \pm 0.044(\text{stat}) \pm 0.026(\text{syst}), \quad (8)$$

which is consistent both with the SM prediction and no asymmetry. Although the systematic errors in the branching fractions are almost as large as the statistical errors, the systematic errors largely cancel in Δ_{0+} .

If we allow the B^+ to B^0 production ratio (f_+/f_0) to deviate from unity, the value of Δ_{0+} shifts approximately by $\frac{1}{2}(f_+/f_0 - 1)$. The value of $f_+/f_0 = 1.044 \pm 0.050$ in Ref. [14] gives $\Delta_{0+} = +0.034 \pm 0.044(\text{stat}) \pm 0.026(\text{syst}) \pm 0.025(f_+/f_0)$. The conclusion above is therefore unchanged, although the result is shifted closer to the SM prediction.

SEARCH FOR PARTIAL RATE ASYMMETRY

We define the partial rate asymmetry between CP conjugate modes (except for the $K_S^0\pi^0\gamma$ mode) as

$$\begin{aligned} A_{CP} &= \frac{\Gamma(\bar{B} \rightarrow \bar{K}^*\gamma) - \Gamma(B \rightarrow K^*\gamma)}{\Gamma(\bar{B} \rightarrow \bar{K}^*\gamma) + \Gamma(B \rightarrow K^*\gamma)} \\ &= \frac{1}{1-2w} \times \frac{N(\bar{B} \rightarrow \bar{K}^*\gamma) - N(B \rightarrow K^*\gamma)}{N(\bar{B} \rightarrow \bar{K}^*\gamma) + N(B \rightarrow K^*\gamma)}, \end{aligned} \quad (9)$$

where N is the signal yield, w is the wrong-tag fraction, B indicates either B^0 or B^+ , K^* indicates $K^{*0}(\rightarrow K^+\pi^-)$ or $K^{*+}(\rightarrow K_S^0\pi^+, K^+\pi^0)$, and \bar{B} , \bar{K}^* are their conjugates, respectively.

The wrong-tag fraction is negligible for K^{*+} , and is 0.9% for K^{*0} due to the double mis-identification of π^+ as K^+ and K^- as π^- . The wrong-tag fraction is obtained from the signal MC; we neglect the small error on this fraction.

Possible detector and reconstruction biases are studied with an inclusive K^* sample. We compare the yield of K^* and \bar{K}^* and find no significant difference in $A_{K^*} = \frac{1}{(1-2w)} \frac{N(\bar{K}^*) - N(K^*)}{N(\bar{K}^*) + N(K^*)}$. We conclude there is no bias and assign systematic errors of 0.007 for $K^{*0} \rightarrow K^+\pi^-$ and $K^{*+} \rightarrow K_S^0\pi^+$, and 0.015 for $K^{*+} \rightarrow K^+\pi^0$. The systematic error on the $\mathcal{L}_{\text{cont}}$ and π^0/η veto requirements is

estimated to be 0.007 in A_{CP} from a comparison of the B and \bar{B} subsets of the $B \rightarrow D\pi^-$ control sample.

We divide the data shown in each of Fig. 1(a–c) into CP conjugate modes. We fit the M_{bc} distributions for the six modes separately, using the same fitting procedure used in the branching fraction measurement. The fit results are shown in Fig. 5 and summarized in Table IV. The errors on the yield extraction are assumed to be uncorrelated. By assuming the partial rate asymmetry is equal for charged and neutral B decays, we add the signal yields for B and \bar{B} with a small correction due to the wrong-tag fraction, and obtain

$$A_{CP}(B \rightarrow K^*\gamma) = -0.015 \pm 0.044(\text{stat}) \pm 0.012(\text{syst}). \quad (10)$$

Here the systematic error includes the errors on A_{K^*} , $\mathcal{L}_{\text{cont}}$ and the yield extraction.

CONCLUSIONS

We have presented branching fraction, isospin asymmetry and CP asymmetry measurements for the radiative decay $B \rightarrow K^*\gamma$ using 85.0×10^6 B meson pairs. The branching fraction results are consistent with previous Belle [9] results, and also with the CLEO [10] and BaBar [11] results, with the errors improved by a factor of two. The $K\pi$ mass spectra and the decay helicity angle distribution in the K^* mass region ($|M(K\pi) - M_{K^*}| < 75 \text{ MeV}/c^2$) are consistent with the dominance of $B \rightarrow K^*\gamma$ without other contributions such as $K^*(1410)\gamma$ or non-resonant $K\pi\gamma$ decays. We measure an isospin asymmetry which is consistent with zero; with the current precision, our result agrees with both the SM prediction and new physics scenarios which have the opposite sign. For the partial rate asymmetry between CP conjugate modes, we obtain a result which is also consistent with zero. For both of these asymmetries, the systematic errors are much smaller than the statistical errors, and hence we can expect further improvements with larger data samples.

Acknowledgments

We wish to thank the KEKB accelerator group for the excellent operation of the KEKB accelerator. We acknowledge support from the Ministry of Education, Culture, Sports, Science, and Technology of Japan and the Japan Society for the Promotion of Science; the Australian Research Council and the Australian Department of Education, Science and Training; the National Science Foundation of China under contract No. 10175071; the Department of Science and Technology of India; the BK21 program of the Ministry of Education of Korea and the CHEP SRC program of the Korea Science and

Engineering Foundation; the Polish State Committee for Scientific Research under contract No. 2P03B 01324; the Ministry of Science and Technology of the Russian Federation; the Ministry of Education, Science and Sport of the Republic of Slovenia; the National Science Council and the Ministry of Education of Taiwan; and the U.S. Department of Energy.

* on leave from Fermi National Accelerator Laboratory, Batavia, Illinois 60510

† on leave from Nova Gorica Polytechnic, Nova Gorica

- [1] CLEO Collaboration, R. Ammar *et al.*, Phys. Rev. Lett. **71**, 674 (1993).
- [2] A. Ali and A. Ya. Parkhomenko, Eur. Phys. J. C **23**, 89 (2002); S. Bosch and G. Buchalla, Nucl. Phys. B **621**, 459 (2002).
- [3] A. Kagan and M. Neubert, Phys. Lett. B **539**, 227 (2002).
- [4] S. Kurokawa and E. Kikutani, Nucl. Instrum. Meth. A **499**, 1 (2003).
- [5] Belle Collaboration, A. Abashian *et al.*, Nucl. Instrum. Meth. A **479**, 117 (2002).
- [6] J. E. Gaiser *et al.*, Phys. Rev. D **34**, 711 (1986).
- [7] R. A. Fisher, Annals Eugen. **7**, 179 (1936).
- [8] The Fox-Wolfram moments were introduced in G. C. Fox and S. Wolfram, Phys. Rev. Lett. **41**, 1581 (1978).
- [9] Belle Collaboration, K. Abe *et al.*, Belle-CONF-0239, “Measurement of the $B \rightarrow K^*\gamma$ Branching Fractions” (2002).
- [10] CLEO Collaboration, T. E. Coan *et al.*, Phys. Rev. Lett. **84**, 5283 (2000).
- [11] BaBar Collaboration, B. Aubert *et al.*, Phys. Rev. Lett. **88**, 101805 (2002).
- [12] ARGUS Collaboration, H. Albrecht *et al.*, Phys. Lett. B **229**, 304 (1989).
- [13] Belle Collaboration, S. Nishida *et al.*, Phys. Rev. Lett. **89**, 231801 (2002).
- [14] Heavy Flavor Averaging Group (URL: <http://www.slac.stanford.edu/xorg/hfag/>).
- [15] K. Hagiwara *et al.*, Phys. Rev. D **66**, 010001 (2002) and 2003 off-year partial update for the 2004 edition available on the PDG WWW pages (URL: <http://pdg.lbl.gov/>).
- [16] A. Kagan and M. Neubert, Eur. Phys. J. C **7**, 5 (1999).

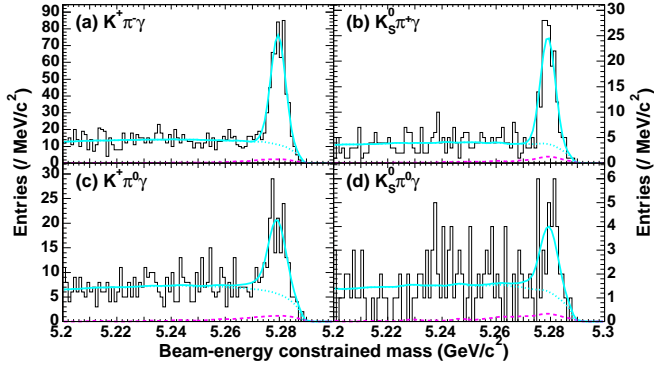


FIG. 1: Fit results for the beam-energy constrained mass distribution for the (a) $K^+\pi^-\gamma$, (b) $K_S^0\pi^+\gamma$, (c) $K^+\pi^0\gamma$, and (d) $K_S^0\pi^0\gamma$ modes. The sum of the signal and the background components are shown in the solid curves, while the dotted and dashed curves represent the total backgrounds and the B decay backgrounds, respectively.

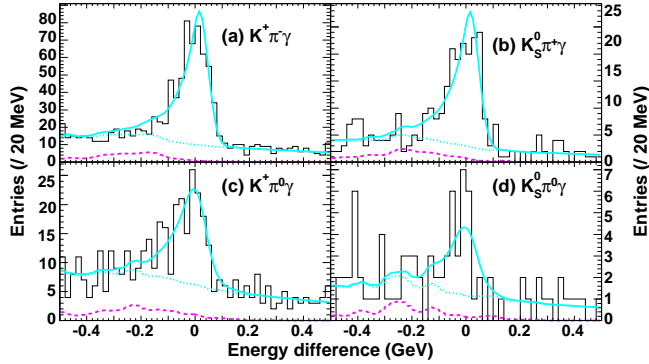


FIG. 2: Fit results for the ΔE distributions. The sum of the signal and the background components are shown in the solid curves, while the dotted and dashed curves represent the total backgrounds and the B decay backgrounds, respectively.

TABLE I: Summary of the signal yields.

Mode	M_{bc}	ΔE	$M(K\pi)$
$K^+\pi^-\gamma$	$450.1 \pm 24.2 \pm 6.1$	453.2 ± 27.4	
$K_S^0\pi^0\gamma$	$23.8 \pm 6.4 \pm 1.0$	23.2 ± 6.2	
$K_S^0\pi^+\gamma$	$145.0 \pm 13.7 \pm 3.6$	147.8 ± 15.4	
$K^+\pi^0\gamma$	$129.1 \pm 14.7 \pm 5.5$	120.0 ± 14.8	
$K^{*0}\gamma$	$473.9 \pm 25.0 \pm 6.2$	476.4 ± 28.1	480.6 ± 25.7
$K^{*+}\gamma$	$274.1 \pm 20.1 \pm 6.6$	267.8 ± 21.4	270.9 ± 19.9

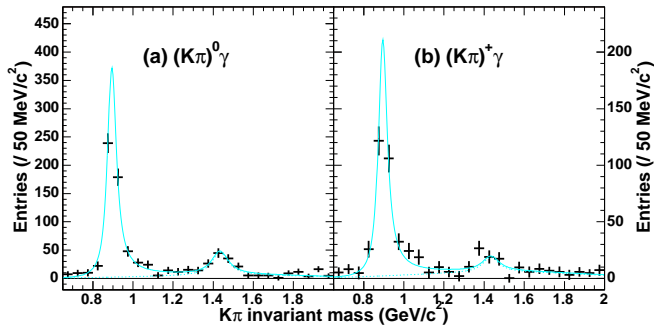


FIG. 3: Fit results for the $K\pi$ invariant mass distributions for the (a) sum of $K^+\pi^-\gamma$ and $K_S^0\pi^0\gamma$, and (b) sum of $K_S^0\pi^+\gamma$ and $K^+\pi^0\gamma$ channels. The sum of the signal and the background components are shown in the solid curves, while the dotted curves represent the background components.

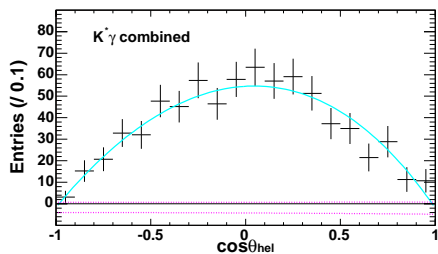


FIG. 4: Fit results for the cosine of the helicity angle ($\cos \theta_{\text{hel}}$) distribution for the sum of all four $B \rightarrow K^*\gamma$ channels. The solid line shows the sum of the signal and the flat component; the $\pm 1\sigma$ bounds of the latter component are shown as the dotted lines.

TABLE II: Reconstruction efficiencies and their systematic uncertainties.

	$K^+\pi^-\gamma$	$K_S^0\pi^+\gamma$	$K^+\pi^0\gamma$	$K_S^0\pi^0\gamma$
Reconstruction efficiency	$(12.83 \pm 0.54)\%$	$(3.96 \pm 0.25)\%$	$(3.63 \pm 0.19)\%$	$(1.09 \pm 0.07)\%$
Fractional errors	4.2%	6.3%	5.3%	6.8%
Number of B meson pairs	0.6%	0.6%	0.6%	0.6%
Photon selection	2.2%	2.2%	2.2%	2.2%
Tracking	2.0%	1.0%	1.0%	—
K^+ identification	0.3%	—	0.3%	—
π^- identification	0.3%	0.3%	—	—
K_S^0	—	4.5%	—	4.5%
π^0	—	—	2.7%	2.7%
$\mathcal{L}_{\text{cont}} + \pi^0/\eta$ veto	1.8%	1.8%	1.8%	1.8%
$M(K\pi)$	1.8%	1.8%	1.8%	1.8%
Non-resonant	1.3%	2.4%	2.4%	1.3%
MC statistics	0.7%	1.2%	1.5%	2.4%

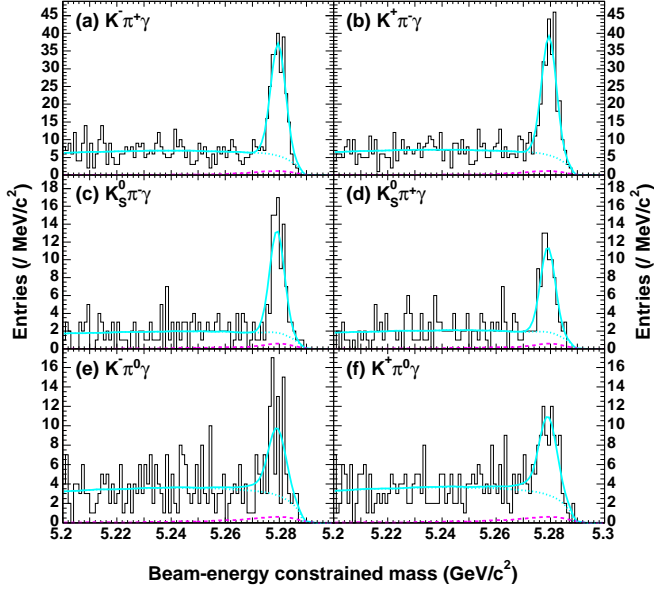


FIG. 5: Fit results for the beam-energy constrained mass distributions for the search for partial rate asymmetry. The sum of the signal and the background components are shown in the solid curves, while the dotted and dashed curves represent the total backgrounds and the B decay backgrounds, respectively.

TABLE III: Results for the signal yields, efficiencies and branching fractions (\mathcal{B}).

	signal yield	efficiency	$\mathcal{B} (\times 10^{-5})$
$K^{*0}\gamma$	$473.9 \pm 25.0 \pm 6.2$	13.92 ± 0.58	$4.01 \pm 0.21 \pm 0.17$
$K^{*+}\gamma$	$274.1 \pm 20.1 \pm 6.6$	7.59 ± 0.39	$4.25 \pm 0.31 \pm 0.24$
$(K^+\pi^-)\gamma$	$450.1 \pm 24.2 \pm 6.1$	12.83 ± 0.54	$4.13 \pm 0.22 \pm 0.18$
$(K_S^0\pi^0)\gamma$	$23.8 \pm 6.4 \pm 1.0$	1.09 ± 0.07	$2.57 \pm 0.69 \pm 0.20$
$(K_S^0\pi^+)\gamma$	$145.0 \pm 13.7 \pm 3.6$	3.96 ± 0.25	$4.31 \pm 0.41 \pm 0.29$
$(K^+\pi^0)\gamma$	$129.1 \pm 14.7 \pm 5.5$	3.63 ± 0.19	$4.19 \pm 0.48 \pm 0.28$

TABLE IV: Results of the partial rate asymmetry search.

K^* mode	$N(\bar{B} \rightarrow \bar{K}^*\gamma)$	$N(B \rightarrow K^*\gamma)$	A_{CP}
$K^{*0} \rightarrow K^+\pi^-$	$218.5 \pm 16.8 \pm 3.0$	$231.6 \pm 17.4 \pm 3.0$	$-0.030 \pm 0.055 \pm 0.014$
$K^{*+} \rightarrow K_S^0\pi^+$	$79.2 \pm 10.0 \pm 1.9$	$65.8 \pm 9.4 \pm 1.9$	$+0.094 \pm 0.094 \pm 0.021$
$K^{*+} \rightarrow K^+\pi^0$	$68.7 \pm 11.6 \pm 2.2$	$80.1 \pm 12.4 \pm 2.5$	$-0.078 \pm 0.113 \pm 0.028$
Combined (K^{*+})			$+0.007 \pm 0.074 \pm 0.017$
Combined (all)			$-0.015 \pm 0.044 \pm 0.012$